Spatially-distributed seasonal and annual geodetic mass balances of Wolverine Glacier, Alaska

Lucas Zeller[1], Daniel McGrath[1], Louis Sass[2], Shad O'Neel[3], Christopher McNeil[2], Emily Baker[2]

1. Department of Geosciences, Colorado State University, Fort Collins, Colorado, USA

2. U.S. Geological Survey Alaska Science Center, Anchorage, AK, USA

3. U.S. Army Engineer Research and Development Center, Cold Regions Research and Engineering Laboratory, Hanover, NH, USA

Correspondence: Lucas Zeller - Lucas.Zeller@colostate.edu

Supplementary Material

Disclaimer: Any use of trade, firm, or product names is for descriptive purposes only and does not imply endorsement by the U.S. Government.

Table S1. Acquisition platform of all 12 DEMs used. All dates are listed in mm/dd/yyyy format

DEM date	DEM platform
09/13/1972	aerial SfM
08/03/1979	aerial SfM
09/27/1995	aerial SfM
09/17/2008	satellite photogrammetry (classified)
08/22/2012	satellite photogrammetry (Worldview)
08/13/2015	aerial SfM
05/05/2016	aerial lidar
09/10/2016	aerial lidar
05/05/2017	aerial SfM
09/12/2018	satellite photogrammetry (Worldview)
09/20/2019	aerial lidar
05/02/2020	aerial lidar

Table S2. Uncertainties related to DEM vertical alignment when stable, snow-free ground is present

Timeframe	$\sigma_{\Delta z}$ (m)	Years	σ_{thin} (m yr^{-1})
2015–16	0.49	1	NaN
2018–19	1.07	1	NaN
1972–95	2.37	23	0.10
1972–79	3.08	7	0.44
2008–12	1.61	4	0.40
2015–19	0.84	4	0.21

Table S3. Glacier-wide mass balance comparison, as in Figure 8

Method	2016 Winter	2017 Winter	2020 Winter	2016 Annual	2019 Annual	2016 Summer
GPR emergence	3.49	2.23	2.34	-0.21	-1.74	-3.69
Profile emergence	3.40	2.17	2.27	-0.44	-2.03	-3.84
Glaciological	3.73	1.66	1.47	-0.14	-1.47	-3.87

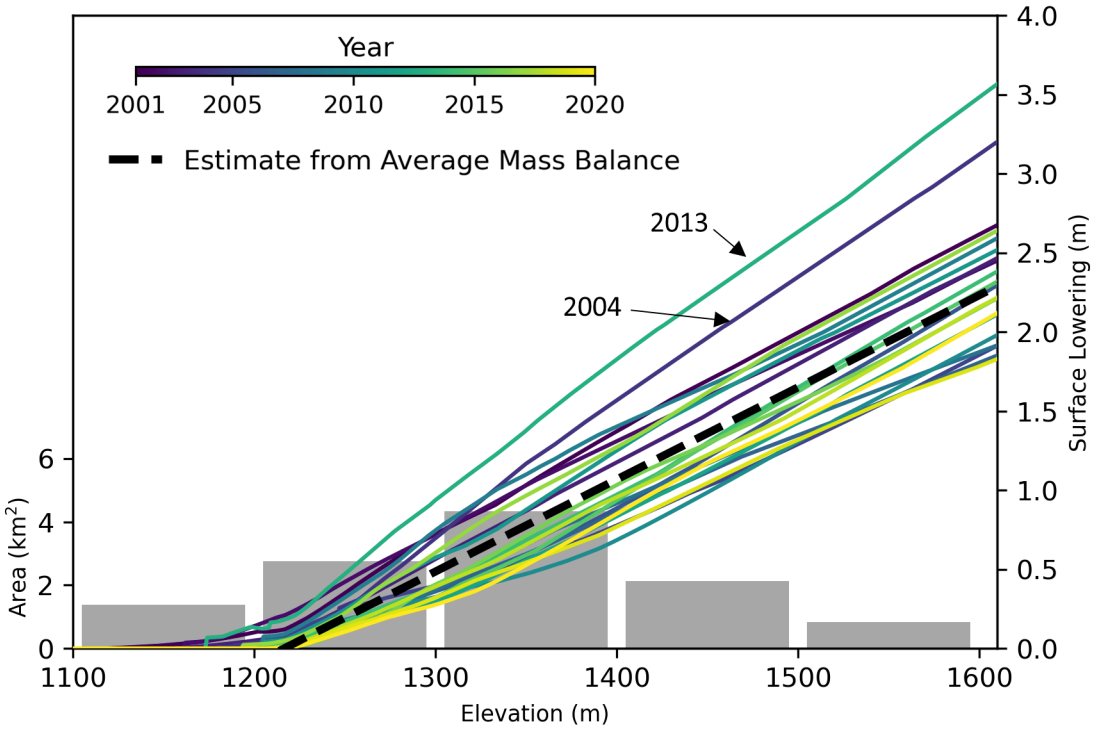

Fig. S1. Elevation profiles of surface lowering due to firn compaction in each of the past 20 years (2001 to 2020) are shown. Dashed black line shows expected firn surface lowering calculated from the modelling approach using the average mass balance over the 20-year time period, as described in Sold et al. (2013). Dark grey bars show the distribution of glacier surface area within 100 m contours (left axis).

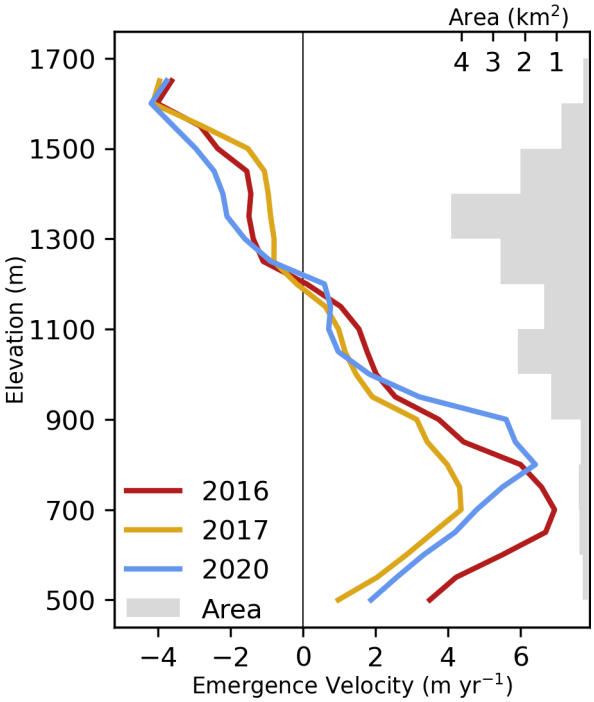

Fig. S2. Elevation profiles of *GPR* emergence velocities in each year displayed as the median value in 50 m elevation bands. Grey bars (right y-axis) show the distribution of glacier surface area within 100 m elevation bands.

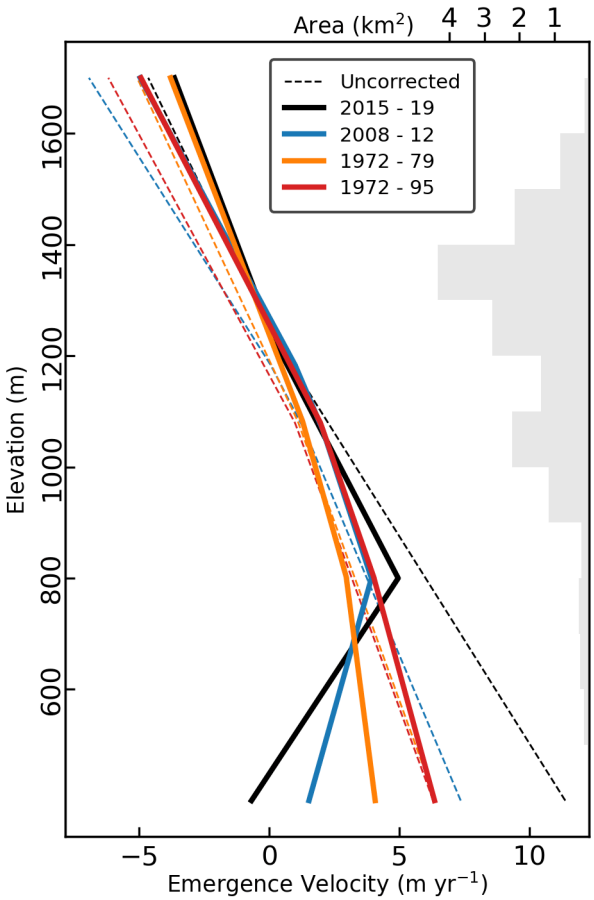

Fig. S3. *Profile* emergence velocities calculated over different timeframes. Dashed lines are uncorrected for glacier thinning, and thick lines are corrected for thinning and with a constant value added such that glacier-wide emergence is equal to zero. Years 2015-19 correspond to the *GPR* and modern *stake* emergence velocities, years 1972-95 correspond to the historical *stake* velocities.

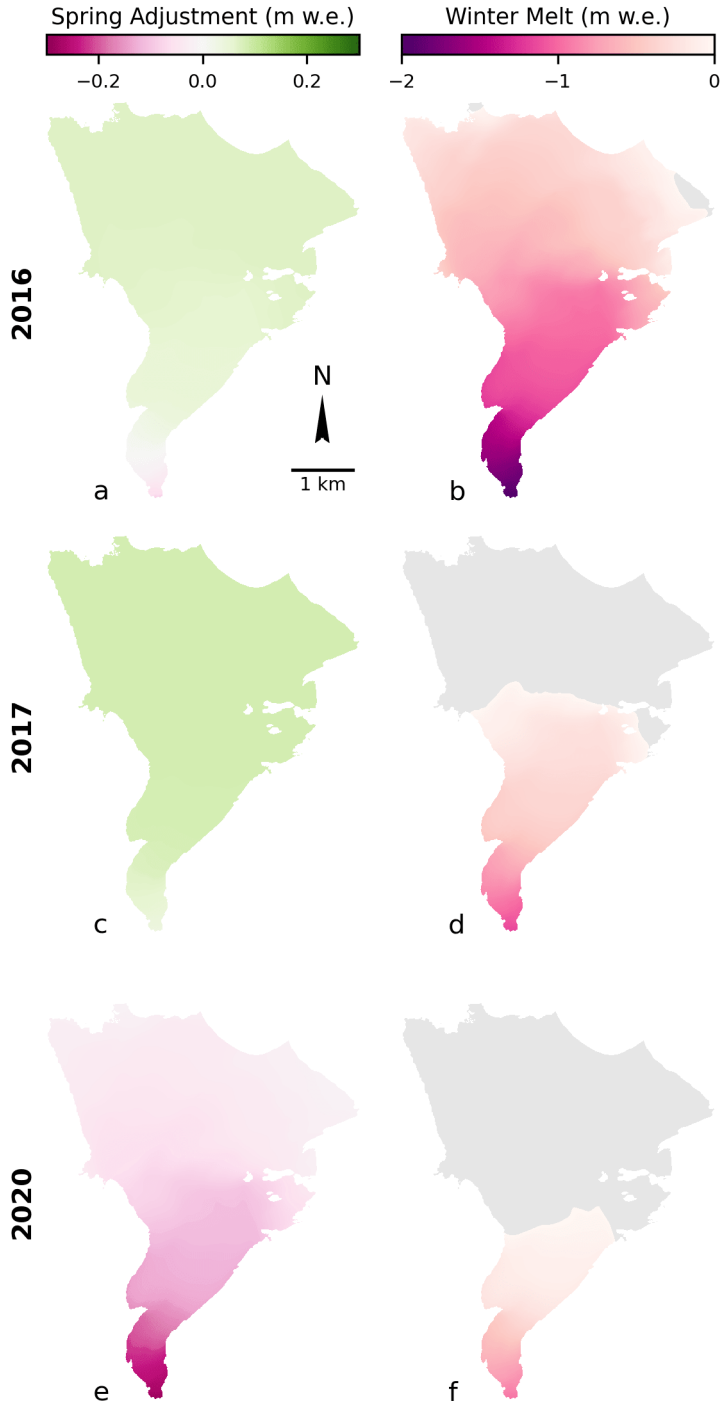

Fig. S4. Surface change due to temporal alignment of ground-penetrating radar and spring DEM surveys (a, c, e) and winter melt occurring after the DEM capture (b, d, f) in each of the three years. These were used as additional inputs in the calculation of *GPR* emergence velocities. Grey areas (b, d, f) indicate no melt occurring.

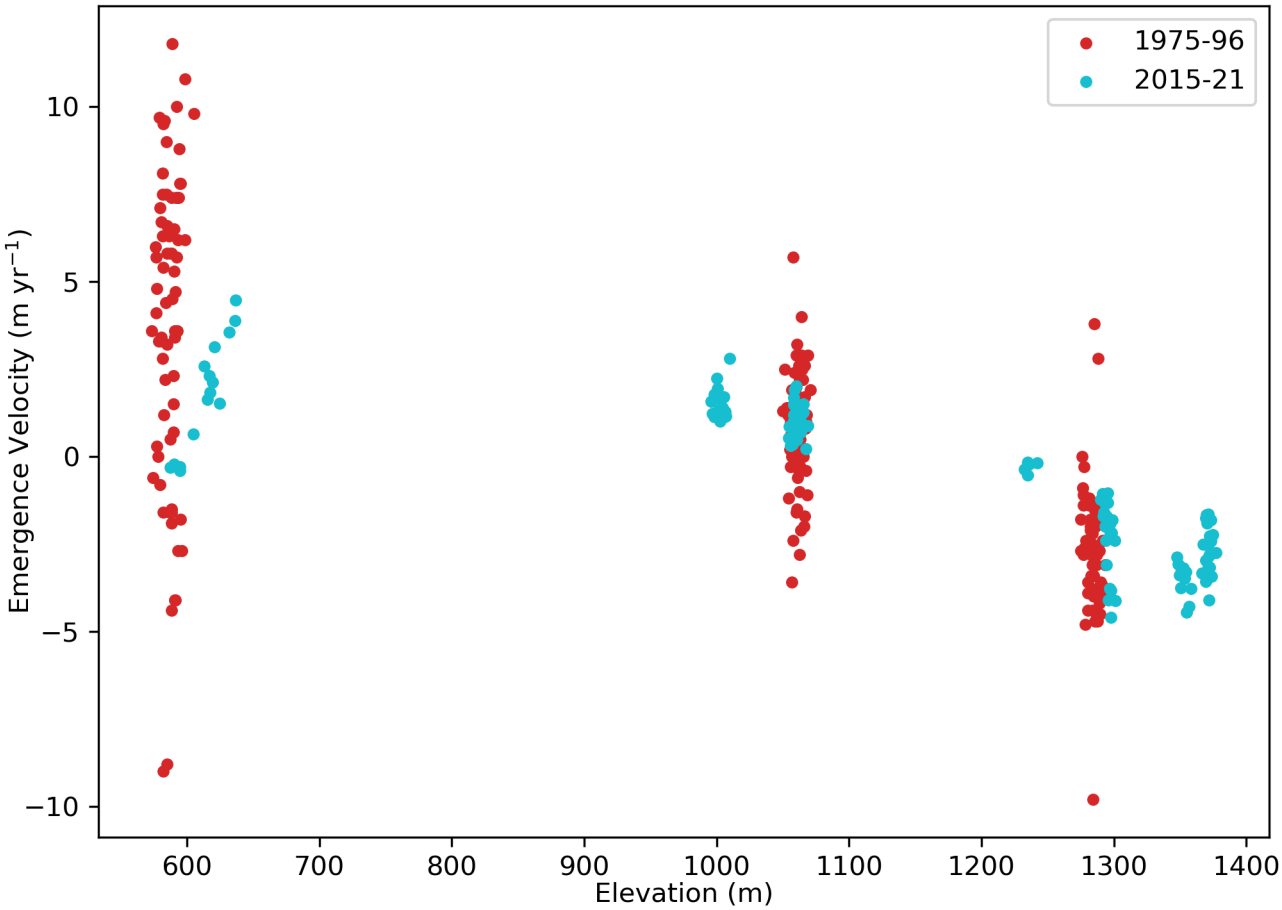

Fig. S5. The distribution of *stake* emergence velocities, plotted according to elevation of the stake. Red dots show measurements from historical stakes (1975-95), and blue shows measurements from modern stakes (2015-21).

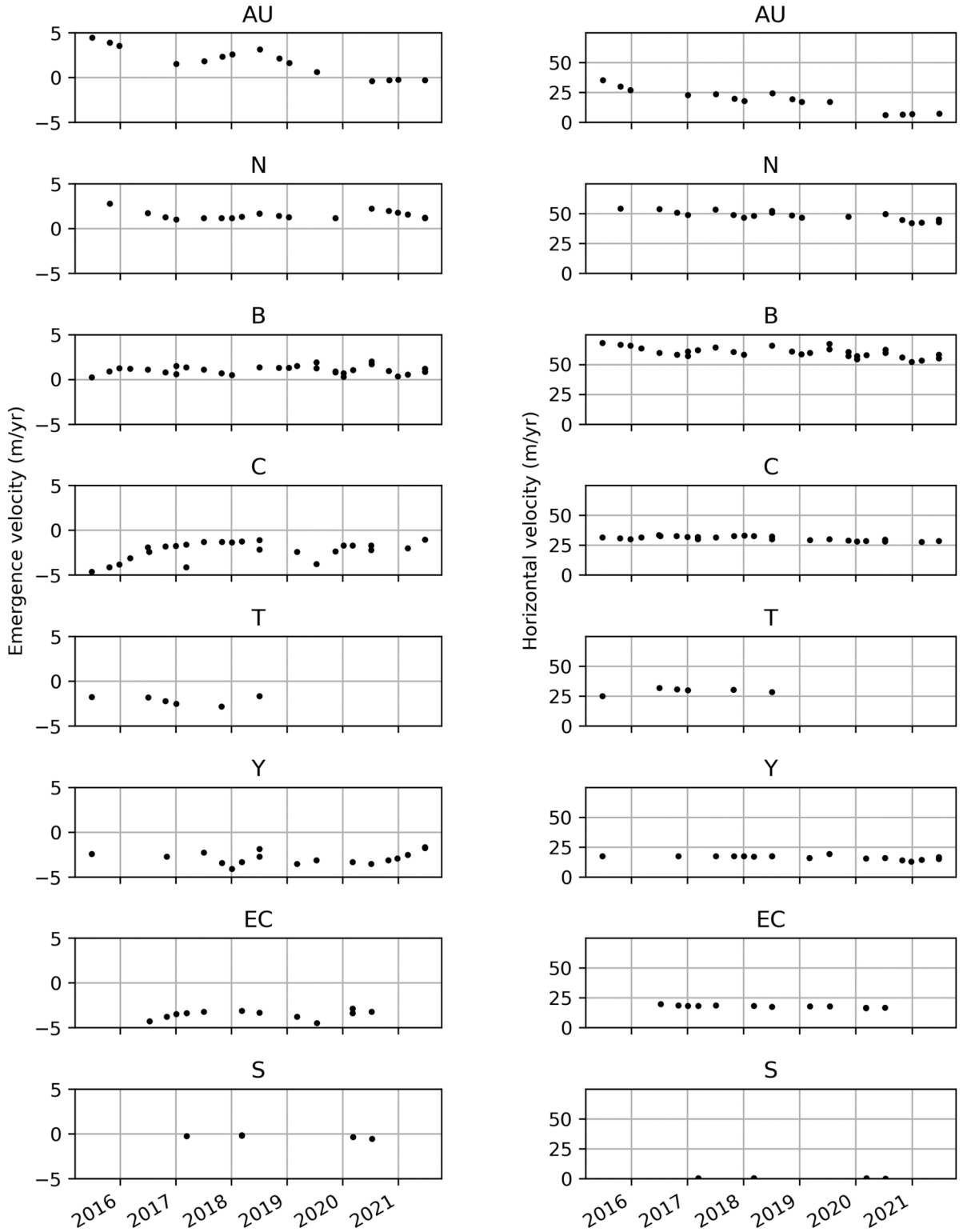

Fig. S6. Time series of horizontal and emergence velocities for each stake in the modern dataset. All plots share the same x-axis. Each point represents a single emergence velocity measurement plotted by middle date between the two stake measurements.

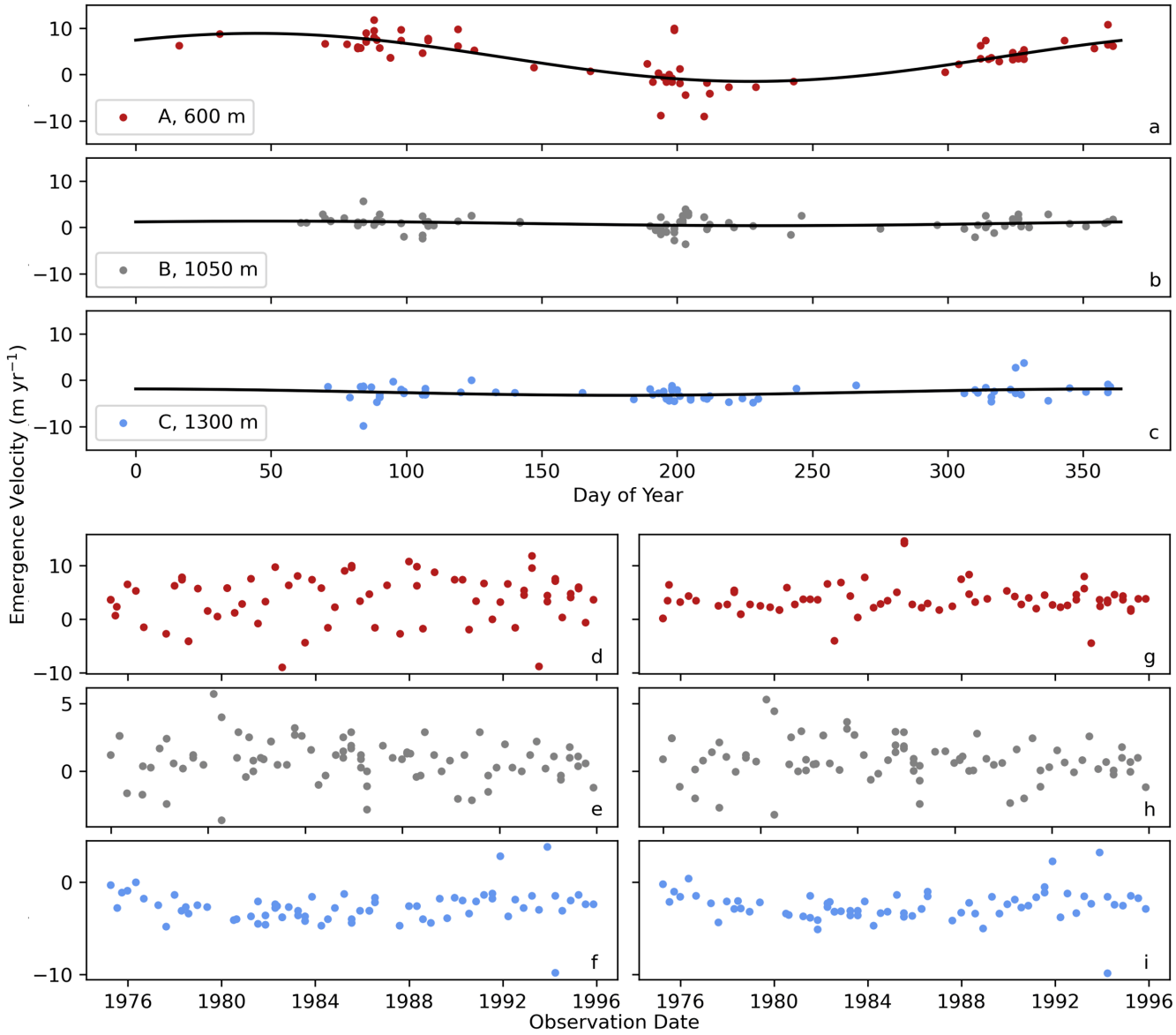

Fig. S7. Seasonality of emergence velocity observed in the historic stake measurements. Stake A (red) is the lowest elevation stake near the terminus, stake B (grey) is near the ELA, and stake C (blue) is the highest elevation in the accumulation zone. Subplots (a-c) show a best-fit sine curve for each stake data, with each point representing a single emergence measurement plotted by the day of year on the x-axis (middle date between the two stake measurements) and emergence velocity on y-axis. Subplots (d-f) show the time series of stake emergence from 1975 to 1995, and (g-i) show the time series corrected for the seasonal variation calculated by the sine curve fit. Seasonality in velocities is clearly visible in stake A, while not as obvious in stakes B and C.

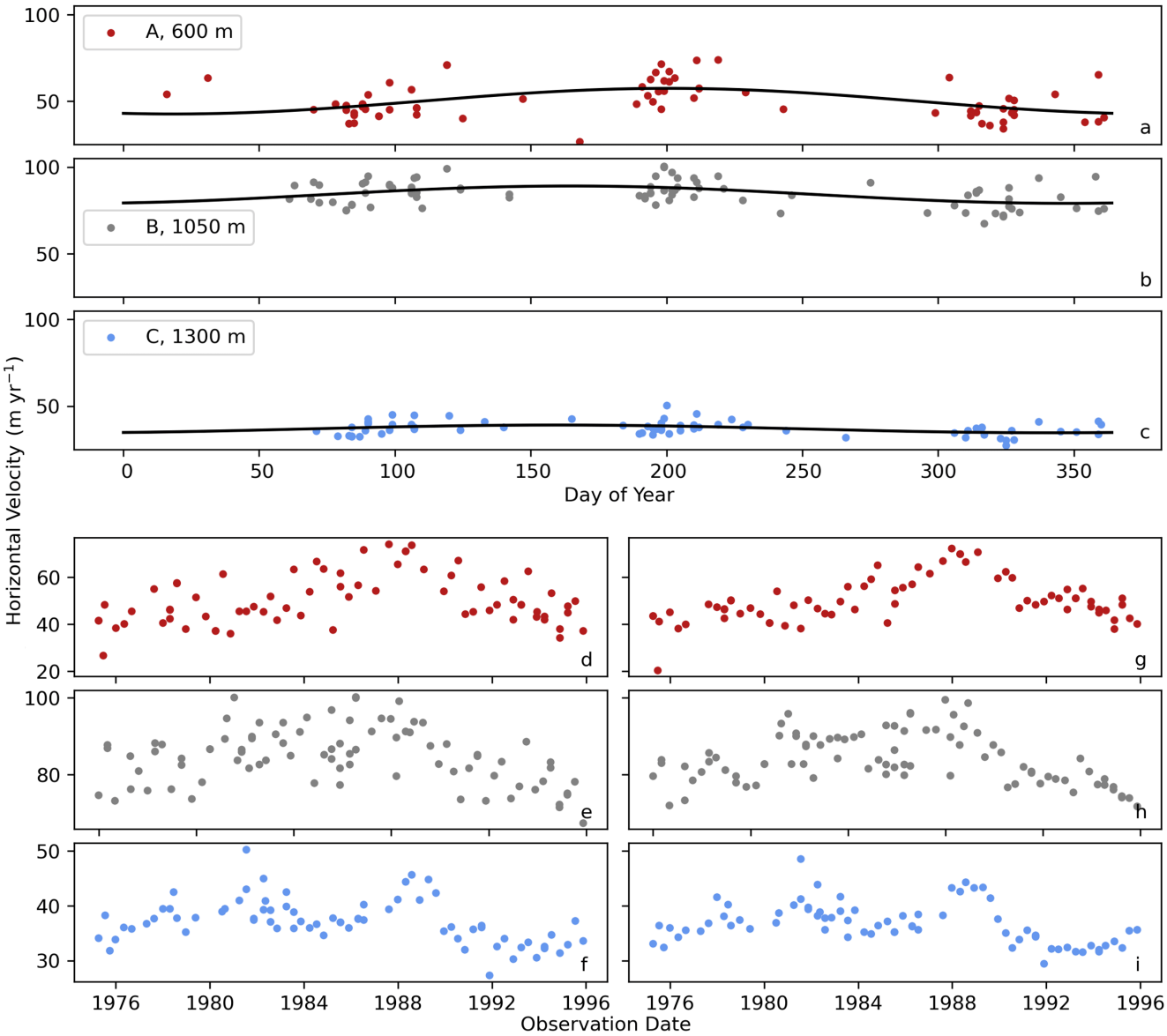

Fig. S8. Like Fig. S7, but for horizontal velocities. Similar to emergence velocities, the seasonality is more pronounced in stake A than stakes B or C.

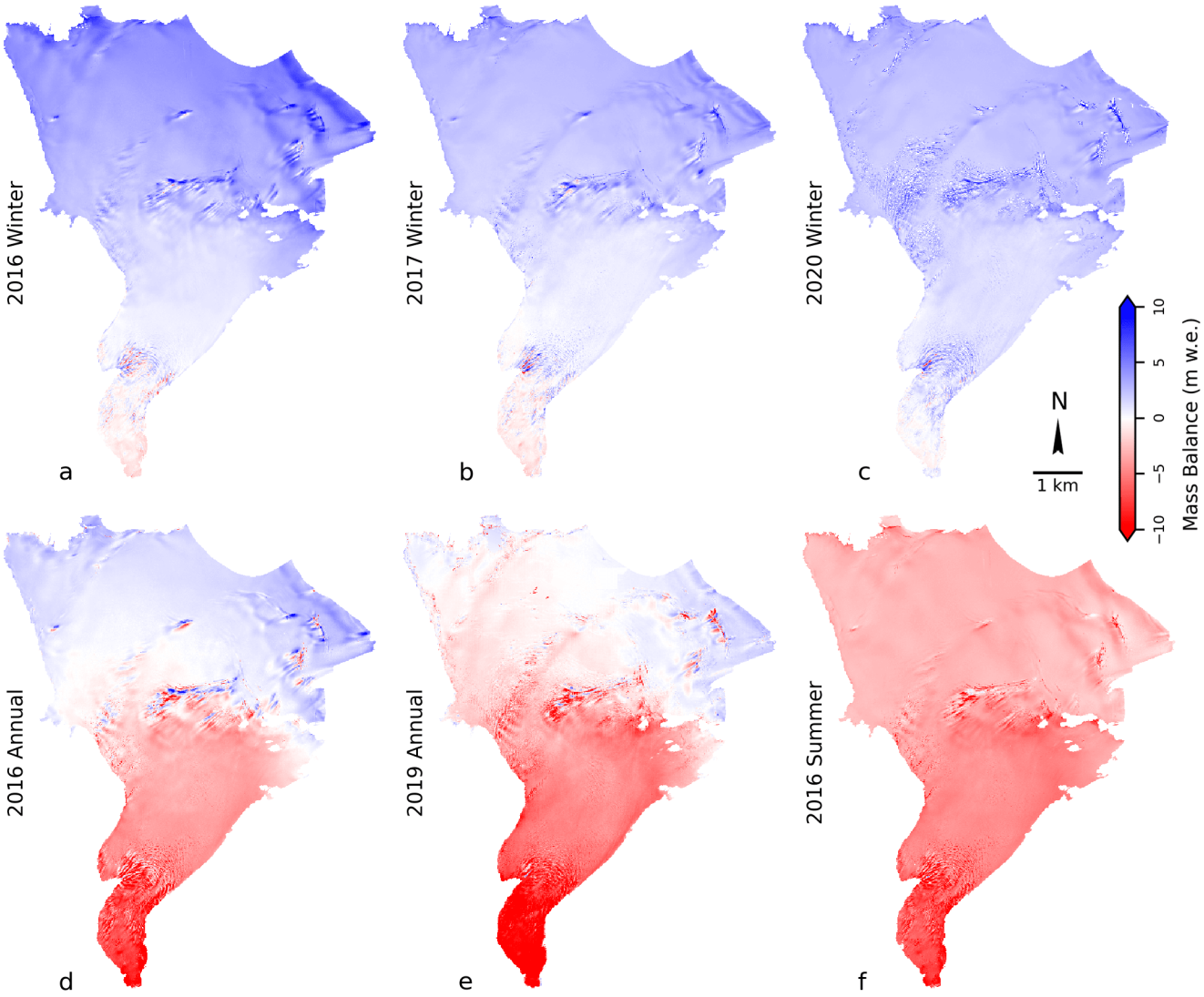

Fig. S9. Distributed mass balances as calculated using the profile approach to account for emergence velocities.

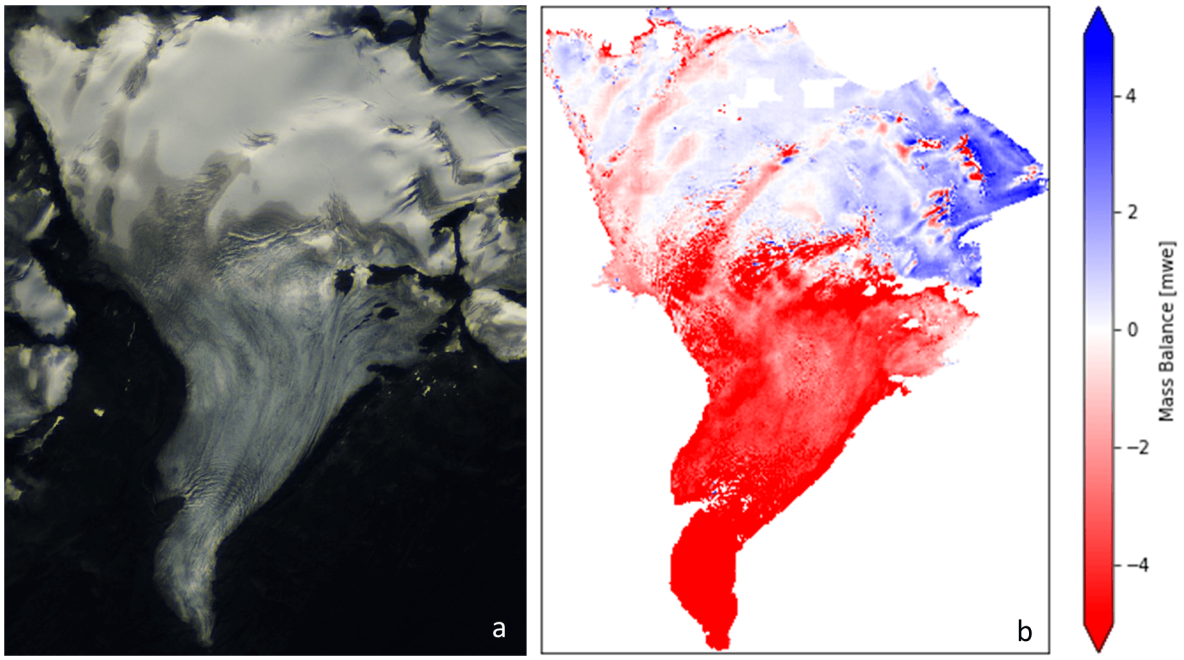

Fig. S10. a) Sentinel-2 satellite image of Wolverine Glacier near the end of summer 2019 (September 14, 2019), coincident with the 2019 fall DEM. The raster values have been stretched to enhance identification of snow (lightest areas in the northern section), firn (grey areas between snow and ice), and ice (dark grey/blue). b) 2019 distributed annual mass balance as calculated in this study, with the colorbar limits condensed to highlight the boundaries between areas of positive and negative mass balance. The distribution of surface types in the Sentinel-2 image matches with the distribution of mass gain and loss, with areas of mass gain coinciding with snow surfaces, and areas of mass loss coinciding with areas of firn and snow.

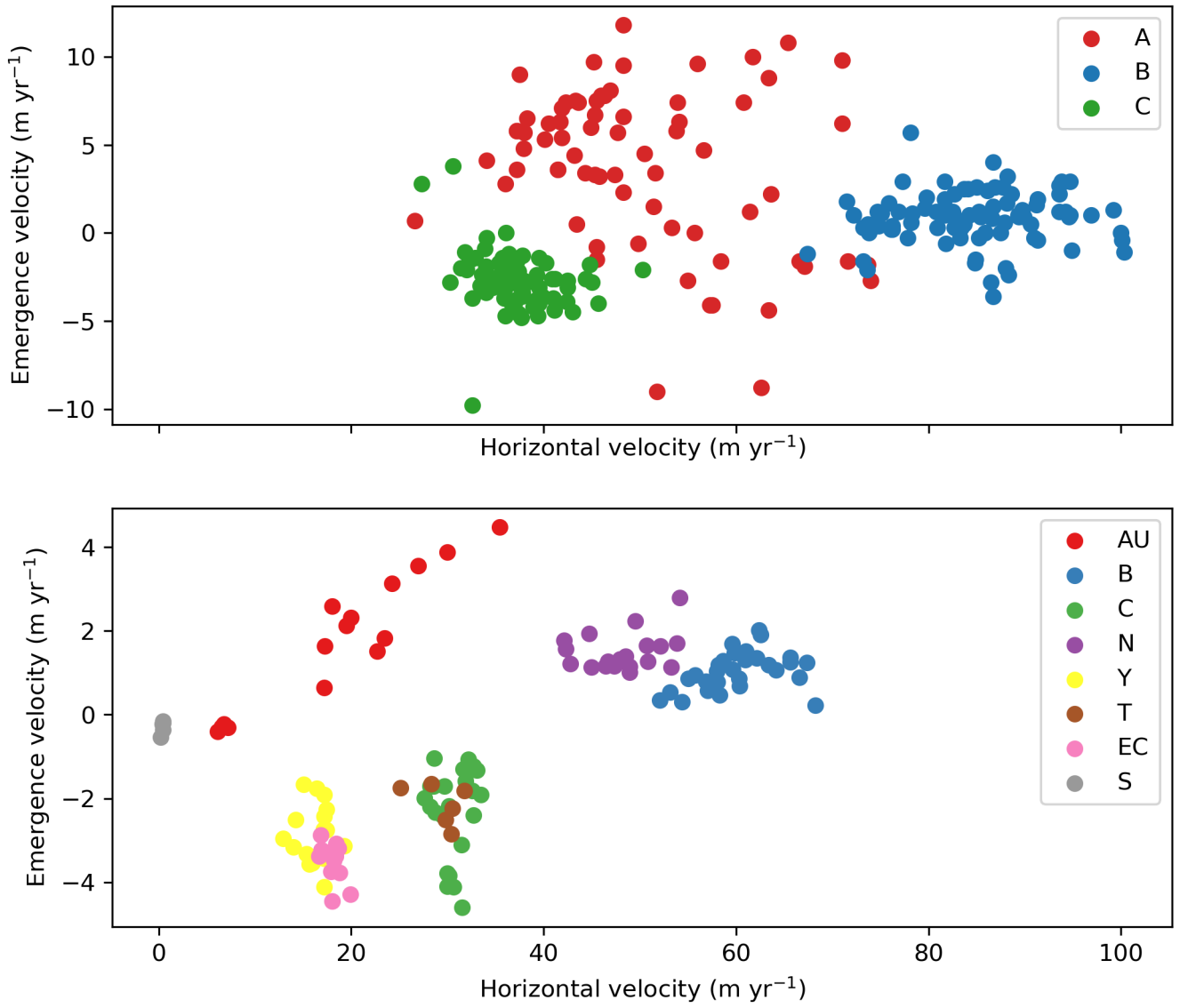

Fig. S11. Coincident horizontal velocities and emergence velocities of historical stakes, showing the lack of significant correlation between the two over coincident timeframes for all but AU ($R^2 < 0.3$ for linear regression for each).

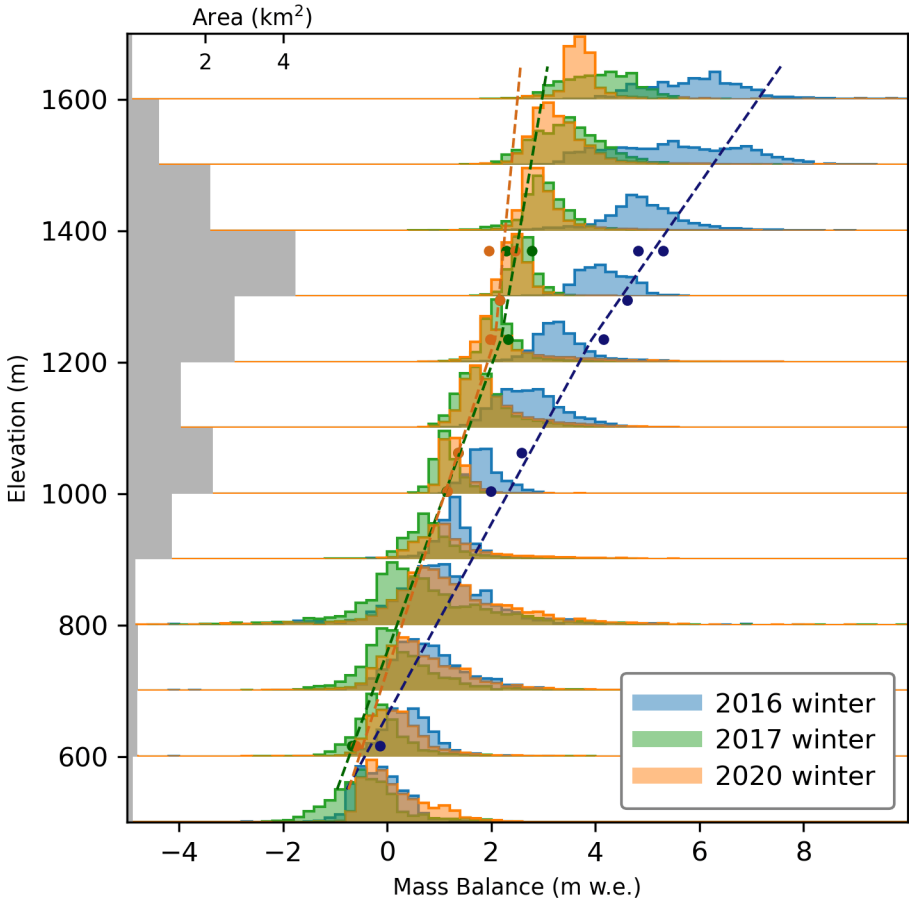

Fig. S12. Winter distributed mass-balance histograms for 2016, 2017, and 2020, from 10x10 m pixels binned within 100 m bands. Histograms are normalized and represent only the relative distribution of balances. Dots show stake-measured mass balances and the corresponding balance profile (dashed lines) from these points. Distributed mass balances were calculated using *profile* emergence constraints and have been temporally aligned with the dates of the stakes and balance profiles.

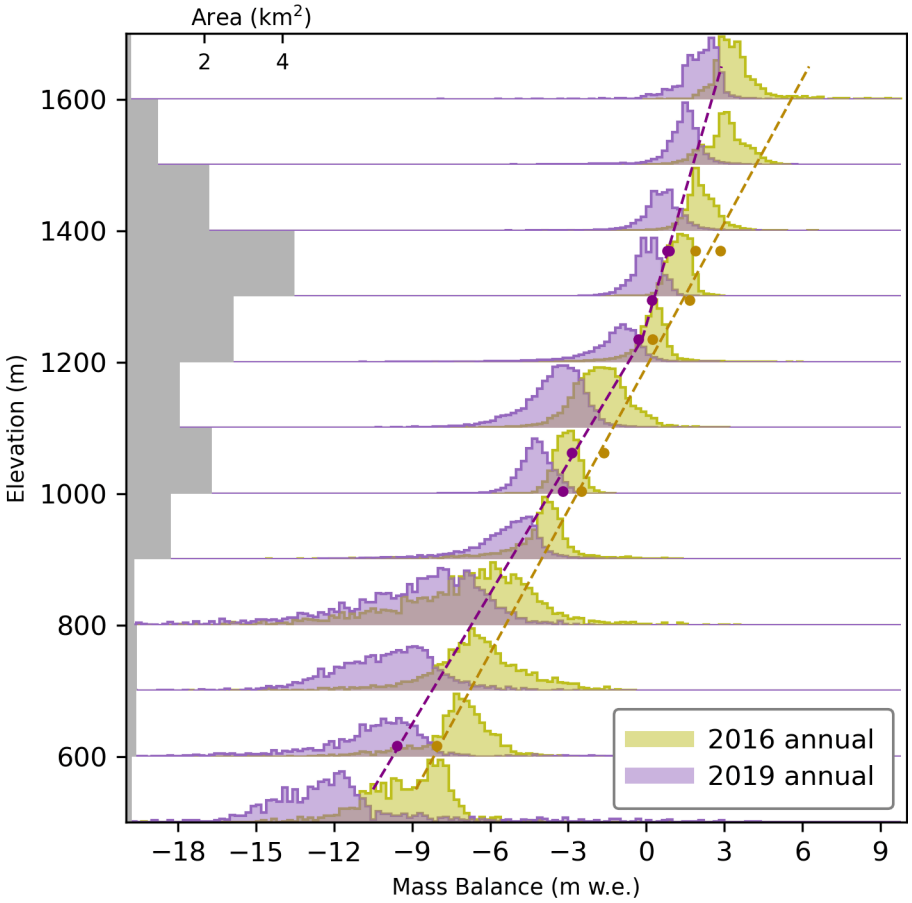

Fig. S13. Annual distributed mass-balance histograms for 2016, 2017, and 2020, from 10x10 m pixels binned within 100 m bands. Histograms are normalized and represent only the relative distribution of balances. Dots show stake-measured mass balances and the corresponding balance profile (dashed lines) from these points. Distributed mass balances were calculated using *profile* emergence constraints and have been temporally aligned with the dates of the stakes and balance profiles.